

Grant Agreement Number:
641185

Action acronym:
CEMCAP

Action full title:
CO₂ capture from cement production

Type of action:
H2020-LCE-2014-2015/H2020-LCE-2014-1

Starting date of the action: 2015-05-01
Duration: 42 months

D7.3

Oxyfuel CFD burner and large kiln simulations

Due delivery date: 2017-10-31
Actual delivery date: 2018-01-23

Organization name of lead participant for this deliverable:
SINTEF Energi AS

Project co-funded by the European Commission within Horizon2020		
Dissemination Level		
PU	Public	X
CO	Confidential, only for members of the consortium (including the Commission Services)	

Deliverable number:	D7.3
Deliverable title:	Oxyfuel CFD burner and large kiln simulations
Work package:	WP7: Oxy-fuel burner technology
Lead participant:	SINTEF-ER

Authors		
Name	Organisation	E-mail
Mario Ditaranto*	SINTEF-ER	mario.ditaranto@sintef.no
Jørn Bakken	SINTEF-ER	jorn.bakken@sintef.no
Mette Bugge	SINTEF-ER	mette.bugge@sintef.no
Francisco Carrasco	University of Stuttgart	francisco.carrasco@ifk.uni-stuttgart.de
Eike Willms	Thyssenkrupp	eike.willms@thyssenkrupp.com
Jamali Armin	VDZ	armin.jamali@vdz-online.de
Ruppert, Johannes	VDZ	johannes.ruppert@vdz-online.de

*Lead author

Keywords
Oxy-fuel combustion; Cement rotary kiln; CFD

Abstract
<p>Oxy-fuel combustion in cement kilns is one of the capture technologies investigated in the CEMCAP Project. The present deliverable reports on optimization of a full-scale rotary kiln operating in oxy-fuel mode by using Computational Fluid Dynamics (CFD) and interaction with process simulation. An optimization procedure and a set of constraints have been defined and followed. The oxy-fuel flame is investigated at different input flow conditions at the burner and secondary gas stream from the clinker cooler, with the objective of reproducing a heat radiation profile to the clinker which is as close as possible to the BAT air reference case defined in CEMCAP. An acceptable trade-off has been found between kiln gas inlet conditions (composition and flow rates) and the boundary constraints imposed to the kiln in terms of hardware, process flow, and heat radiation to the clinker. The ThyssenKrupp designed POLFLAME burner has demonstrated to be able to generate an oxy-fuel flame with similar heat transfer characteristics in air and oxy-fuel requiring only to adapt the modulable swirl angle of the burner high velocity nozzles. Retrofit applications and air/oxy-fuel mode shifting are therefore possible without changing the burner. The study has shown the particular features of flame stabilization pattern with this burner and highlighted the rotary kiln characteristics that were most sensitive to the flame properties.</p>

Please cite this report as: *Ditaranto Mario, Bakken Jørn, 2017. Oxyfuel CFD burner and large kiln simulations (D7.3)*. Refer to the [CEMCAP community in Zenodo.org](#) for citation with DOI.

TABLE OF CONTENTS

	Page
1 INTRODUCTION	1
2 VALIDATION OF CFD MODEL WITH PILOT PLANT TESTING.....	2
2.1 Introduction	2
2.2 Numerical Setup	2
2.3 Numerical results.....	4
2.4 Conclusions of the validation study.....	9
3 METHODOLOGY FOR THE OPTIMIZATION PROCEDURE.....	11
4 NUMERICAL SETUP	14
4.1 Cement rotary kiln CFD model	14
4.2 Fuel and combustion model.....	15
5 RESULTS AND DISCUSSION	18
5.1 Flame dimension	19
5.2 Flame radiation properties	20
5.3 Near burner flame characteristics	21
5.4 Discussions	24
6 CONCLUSIONS AND FURTHER WORK.....	26
7 REFERENCES	28

1 INTRODUCTION

Oxy-fuel combustion in cement kilns is one of the capture technologies investigated in the CEMCAP project. The technology is based on combustion with oxygen and recirculated flue gas (mainly CO₂) instead of air. Changing the oxidizer composition has significant impact on the characteristics of the flame developed in the rotary kiln as it affects many physical parameters, but it is important that the heat transfer to the clinker remains the same to maintain product quality and process efficiency. Work Package 7 (WP7) investigates a burner, called POLFLAME from the project partner ThyssenKrupp (TKIS) for operating in oxy-fuel conditions on a full scale 3000 t/d rotary kiln. One challenge is that the burner must be able to cope operation in both air and oxy-fuel modes with only minor hardware modifications that can be done without stopping the process. Since the rotary kiln is only one stage imbricated in the entire clinker production process, the boundary conditions of the gas streams at the rotary kiln input and output must be harmonized. Therefore, the modifications imposed by the oxy-fuel operation to the rotary kiln must be studied in parallel with the overall process simulation (PM) work and the task described in this report is the result of an interaction with WP6 "Oxyfuel modelling and optimization". The investigation of a full-scale rotary kiln fitted with the POFLAME burner is made by Computational Fluid Dynamics (CFD) with a commercial code. Preliminary work in WP7 has validated the CFD setup and methodology against pilot testing performed at the University of Stuttgart with a thermal power input of 500 kW in air and oxy-fuel modes.

2 VALIDATION OF CFD MODEL WITH PILOT PLANT TESTING

2.1 Introduction

A new burner for oxy-fuel conditions has been designed by ThyssenKrupp Industrial Solutions AG (TKIS), which in the CEMCAP project has been downscaled, built, and tested in the 500 kWt combustion test rig at the University of Stuttgart (USTUTT) [1]. Three test campaigns were carried out from which the setup and results from the second test campaign have been used as case for validation of the numerical calculations. Both air and the oxy-fuel cases have been simulated. The results presented herein have been achieved after extensive tests, selection of the models used in the CFD, and meshing of the burner and combustion chamber. This validation stage revealed to be necessary as it allowed to solve issues related to the mesh quality and convergence problems caused by the models used in an oxy-fuel context.

2.2 Numerical Setup

Although the full-scale case uses coal, the pilot experiments were carried out with pet-coke due to fuel availability and time constraints in the project. Details of the test campaigns are described in CEMCAP MS7.6. The properties for the pet-coke used in the calculation are shown in the table below. To simplify the numerical set-up, the small amount of nitrogen in the fuel (1.6%) was removed and compensated by increasing the Sulphur content from 3.2 to 4.8.

The full-scale burner has 10 symmetrical high velocity nozzles (see later section for description of the full-scale burner), but the downscaled version only contains 8 due to manufacturing limitations. Therefore, the numerical model only considers a 45° section to which boundary conditions are periodic. The burner circular nozzle of the primary oxidizer has been modeled as a trapezoid having the same area. The flow from the nozzle was set with 20° swirl angle (axial velocity component 0.939 ($\cos(20^\circ)$), tangential component 0.342 ($\sin(20^\circ)$). All inlets (see Figure 2.1) were set up as mass-flow inlets, while the outlet was set as a pressure outlet.

The mesh is shown in Figure 2.2. To get a Cartesian grid, the center of the combustion chamber (2 cm diameter) was cut off. This is equivalent to having a 2-cm rod in the center of the combustion chamber. The wall shear stresses on this surface was set to zero. The resulting mesh consists of 2,599,000 cells. The wall temperature in the combustion chamber was set by a User Defined Function (UDF) based on the measured temperatures close to the wall. The different models used in the simulations are listed below.

Table 2.1: Models used.

Fluent	Model
Turbulence	k-omega SST
Chemistry	Species transport, Finite rate/Eddy-Dissipation, 6 reactions, ideal gas
Radiation	Discrete Ordinates
Solver	Pressure based with Pseudo-transient model enabled, as well as Higher Order Term Relaxation
Wall temperature	Profile calculated from IFK experiments (UDF)

Properties for the petcoke used in the simulations are listed in Table 2.2. There are some minor divergences from the petcoke used in the experiments. This is due to some inconsistency between fixed carbon and total carbon reported from the experiments, and the above-mentioned substitution of petcoke-nitrogen by sulphur.

Table 2.2: Petcoke properties used in the simulations.

Properties (Units)	Value
HHV (J/kg)	33,000
Volatiles (% by mass)	11.32
Fixed C (% by mass)	82
Ash (% by mass)	2.12
Moisture (% by mass)	4.56
Petcoke size (μm)	5-120
Petcoke temperature (K)	303
Petcoke inlet velocity (m/s)	23
Petcoke feed rate (kg/s/segment)	0.0018
Petcoke ultimate analysis (water and ash free):	
C (% by mass)	87.91
H (% by mass)	3.64
O (% by mass)	3.6
N (% by mass)	0
S (% by mass)	4.85

The inlet flows/parameters are shown in Table 2.3. The cooling gas for the flame detector, and the estimated air entrance, have not been included in the calculations since the location of these inlets was unknown. It is, however, likely that these flows will have some effect, at least on the temperature. For the air case, the cooling air to the flame detector increases the total mass flow (or volume flow) with 3.3%. The additional air entrance is unknown. For the oxy-case, CO_2 for cooling of the flame detector and "Estimated air entrance" increase the total mass flow of gas with 4.4% (5.5% for the volume flow). For the combustion, the model *Species Transport with Eddy Dissipation/Finite Rate* was used. In addition to the default one-step reaction for volatiles, five additional reactions have been included for char burnout:

1. $\text{Volatiles} + 2.01\text{O}_2 \rightarrow 1.2\text{CO}_2 + 2.2\text{H}_2\text{O} + 0.02\text{N}_2 + 0.02\text{SO}_2$
2. $\text{H}_2 + 0.5\text{O}_2 \rightarrow \text{H}_2\text{O}$
3. $\text{CO} + 0.5\text{O}_2 \rightarrow \text{CO}_2$
4. $\text{C(s)} + 0.5\text{O}_2 \rightarrow \text{CO}$
5. $\text{C(s)} + \text{CO}_2 \rightarrow 2\text{CO}$
6. $\text{C(s)} + \text{H}_2\text{O} \rightarrow \text{H}_2 + \text{CO}$

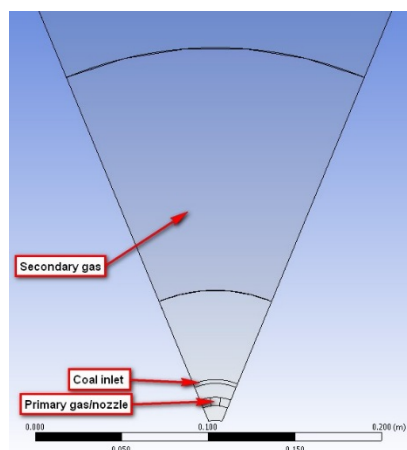


Figure 2.1: Gas inlets in model.

Table 2.3: Inlet conditions in pilot tests ("USTUTT 500") and simulation ("USTUTT 500 CFD").

		USTUTT 500		USTUTT 500 CFD	
		AIR	OXY-FUEL	AIR	OXY-FUEL
Prim + Carr + flame detector					
Volume flow	Nm ³ /h	161	130	131	110
Temperature	K	303	303	303	303
Composition					
N2 or CO2		N2	CO2	N2	CO2
O2 %	Vol. fraction	21.0	34.7	21.0	41.0
N2 or CO2 %		79.0	65.3	79.0	59.0
O2	Nm ³ /h	34	45	27	45
CO2 or N2	Nm ³ /h	127	85	103	65
available combustion O2	g_O2/g_fuel	0.929	1.241	0.755	1.241
Secondary gas					
Volume flow	Nm ³ /h	321	255	321	255
Temperature	K	1013	985	1013	985
Composition					
N2 or CO2		N2	CO2	N2	CO2
O2 %	Vol. fraction	21	21	21	21
N2 or CO2 %	Vol. fraction	79	79	79	79
Velocity	m/s			2.4	1.9
Total gas					
Volume flow	Nm ³ /h	482	385	452	365
Primary/secondary	ratio	0.318	0.333	0.318	0.333
Composition					
N2 or CO2		N2	CO2	N2	CO2
O2 %	Vol. fraction	21	26	21	27
N2 or CO2 %	Vol. fraction	79	74	79	73
O2	Nm ³ /h	101	99	95	99
CO2 or N2	Nm ³ /h	380	286	357	266

2.3 Numerical results

The calculation for pet-coke-air was first run for 12,400 iterations with a single particle size. Then a particle size distribution of 5 - 120 μm was introduced and the calculation run for further 3,600 iterations. The results at 12,400 iterations was also used as a starting point for the oxy-fuel calculation, and run for 2,200 iterations before the particle size distribution was introduced, for then run for further 3,600 iterations. Simulation residuals of species, velocities, and energy which are used as marker for achievement of convergence were used to decide for whether to stop the calculation. Mass flow and the oxygen concentration at the outlet were stable.

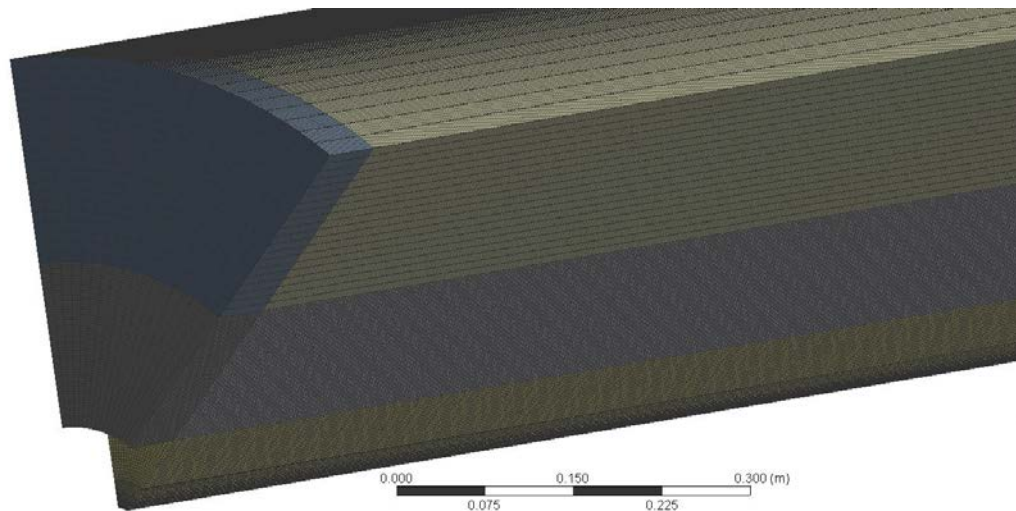


Figure 2.2: Mesh of inlet section and start of combustion chamber.

2.3.1 Species and temperature

Before comparing measured and simulated results of species a comment must be made on the effect of unaccounted volume flows due to detector cooling and leakages (cf. § and Table 2.3), in order to give an idea of the accuracy of the measured data. Table 2.4 shows the values of O₂ concentration measured at the outlet of the boiler and obtained by calculating the mass balance based on the volume flow inputs. The difference is due to leakages either at the boiler limits (windows, flanges, etc.) or in the sampling line. The unknown air flow ingress is estimated to be 15 Nm³/h in the oxy-fuel case, while no estimate is given for the air case. To match the measured O₂ concentration at the outlet in the air case, one has to add 10 Nm³/h.

Table 2.4. Outlet oxygen concentration in boiler test and simulations.

O ₂ (% by vol.)	Air	Oxy-fuel
Measured at boiler outlet	2.2	3.4
Mass balance incl. detector	1.8	1.1
Mass balance incl. detector and estimated leaks	2.2	2.9

Figure 2.3 shows the calculated oxygen concentration compared to the measured concentration. Both for the air case and the oxy-fuel case, a final concentration is reached at a shorter distance from the burner in the CFD simulations than in the experiments, due to the combustion model in the EDM/Finite rate combustion model where the shortest of the eddy dissipation or finite rate timescales is used. In this case with swirling flow, turbulence will be controlling the rate of reaction and therefore give faster reaction. Similar behavior can be seen in CO₂ and CO (Figure 2.4 and Figure 2.5). On the measured CO₂ profiles in Figure 2.4 in oxy-fuel mode it is seen that there is relatively little variation all along the flame and that the measurement uncertainty, estimated by the fluctuations between adjacent points, can vary by almost the same amount as the overall variation in the whole boiler. As a consequence, the measurements cannot capture the strong gradients occurring in the flame region and make the comparison difficult. Besides, we can note an inconsistency in the CO₂ concentration tending to 70 % in the boiler, whereas the monitored CO₂ value at the boiler exit (at ca. 5 m) is 84.6 %, which is closer to the value calculated from a mass balance between inputs and outputs in the boiler. It is difficult to

envisage that the difference of 14.6 %-points between 3.41 m and 5 m could be covered by further completion of combustion when the measured CO values are already so low at 3.41 m, as will be seen later. It is possible that the measured CO₂ concentrations suffered from air leakage during sampling and calibration limitations at high concentration values. This is consistent with the higher measured O₂ concentrations observed in Figure 2.3, therefore these experimental values should be taken with care.

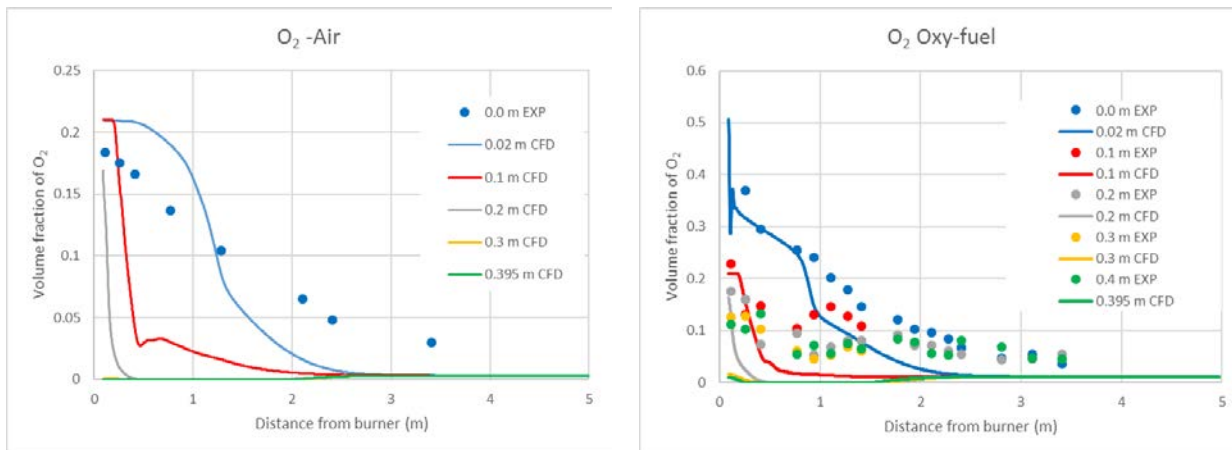


Figure 2.3: Measured and calculated volume fraction of O₂ in air and oxy-fuel cases.

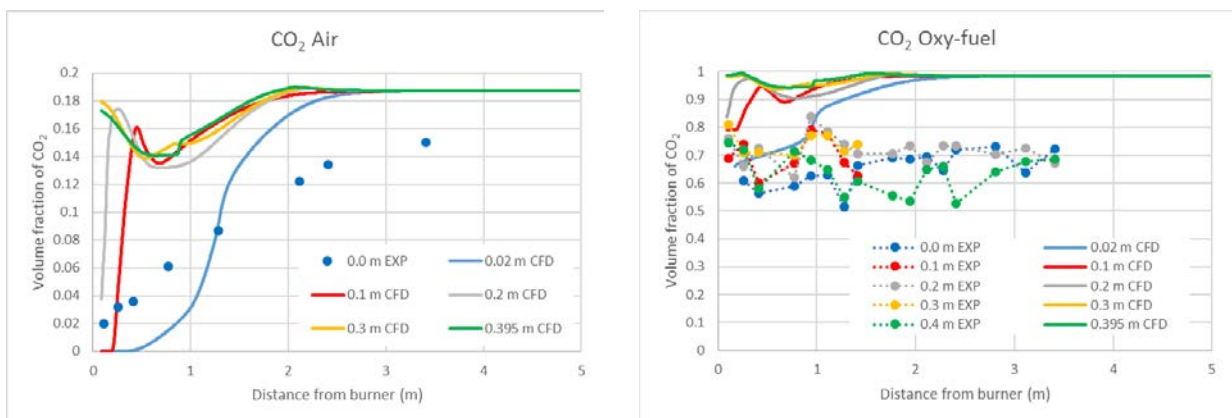


Figure 2.4: Measured and calculated volume fraction of CO₂ in air and oxy-fuel cases.

CO is only measured along the centerline in the air case. However, as the simulations show, this is where the lowest CO concentrations are (Figure 2.5). It is also clearly shown in the contour plot shown as insets in Figure 2.5, that the maximum concentration is outside of the center. The same is also true for H₂.

Both CO and H₂ are intermediate species in the flame zone. The reaction rate of these species (in the reactions above) will affect how fast they are consumed (default reaction rates are used in Fluent). From the comparison with the experiments it is clear that these reactions are too slow for combustion of petcoke. One reason for discrepancies between calculated and measured results is the reduced mechanism which does not take into account the hundreds of intermediate reactions and species actually occurring in solid hydrocarbon fuel combustion and which tend to overestimate the limited number of intermediate species considered here (CO and H₂). All

results show that these intermediate species are produced and consumed within the first two-three meters of the combustion chamber. The reduced reaction mechanism used will cause all char to first be reacted to CO. For petcoke this will lead to locally high concentrations of CO. The reaction rates and activation energy will be changed from the default values in the full-scale simulations. It must be noted that the measured CO concentrations are significantly low. Indeed, solid fuels with low volatile content are prone to produce less CO in comparison to high volatile fuels [2]. High volatile fuels, like lignite usually present very high local concentration of CO (several 10,000's ppm) in near flame region. This effect is even exacerbated in oxy-fuel, where the CO₂ kinetics favors the formation of CO through $\text{CO}_2 + \text{H} \rightleftharpoons \text{CO} + \text{OH}$. This is something SINTEF has observed in several studies on oxy-fuel and also noted in the ECRA CCS Project Phase III, where up to 60,000 ppm CO was observed. Therefore, comparison between simulation and measured CO profiles is difficult, as very specific chemical effects in combustion with low-volatile fuels are not captured by the reduced chemical mechanism used.

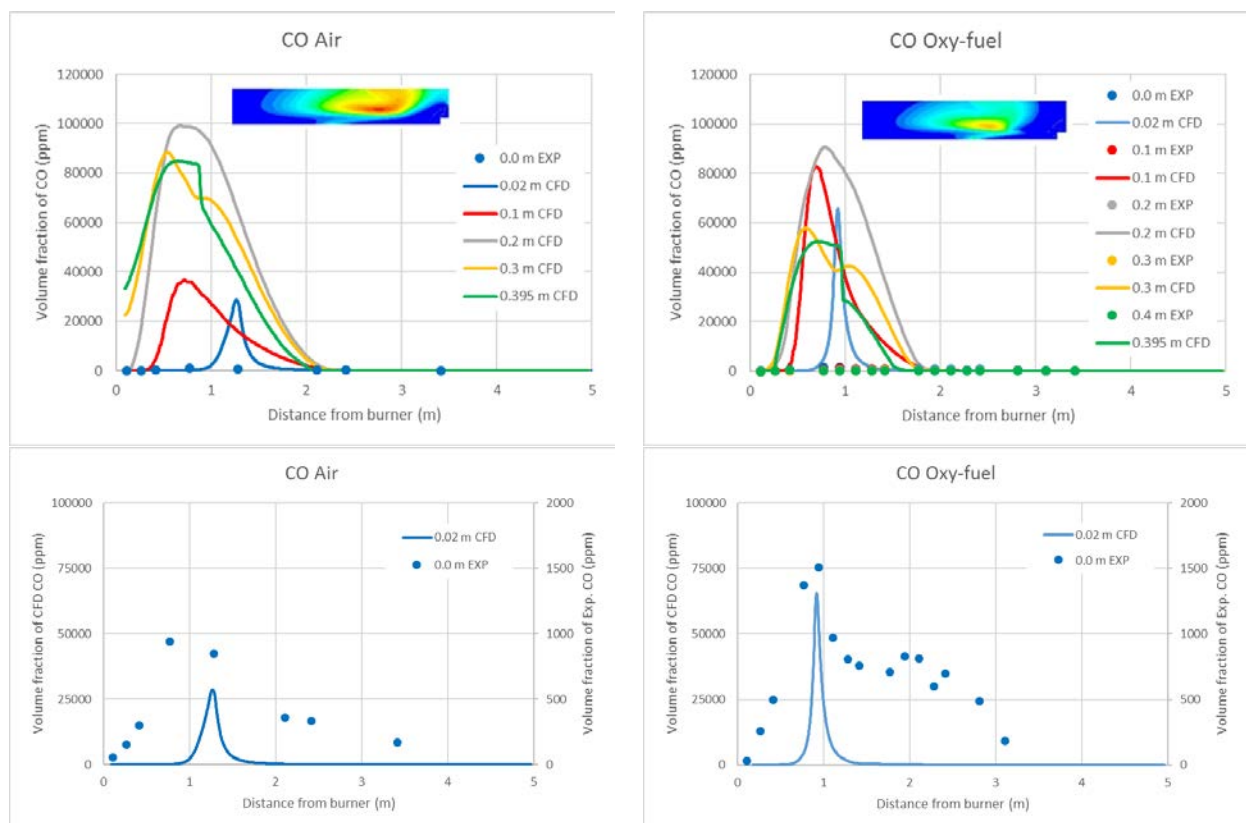


Figure 2.5: Measured and calculated volume fraction of CO in air and oxy-fuel cases.

Streamwise temperature profiles are shown in Figure 2.6 and contour maps are given in Figure 2.8. The maximum temperature measured along the centerline are generally lower than the calculated. One reason is the general faster combustion rate as observed previously in the calculations. The over-estimation of the peak temperature is probably due to the reduced chemical mechanism used and increased mixing. However, it must be noted that the flame detector cooling gas and air leakages on the furnace are not taken into account in the simulations and these have a non-negligible cooling effect on the flame. Indeed, in the oxy-fuel case, this extra flow gas accounts for an additional 18% of the total primary gas and could not be included in the simulations because the furnace modelled does not have the flame detector and the air leakages inlets. For the air case the leakage air flow is not estimated, but if the same amount as

in oxy-fuel is considered it accounts for an extra 23 % of the total primary flow. The temperature measured in the air case along the centerline is around 1300 K, which seem quite low for such a flame. In similar configuration of heat load and in the same installation, measured temperatures were over 1600 K (cf. first validation dataset in CEMCAP project). Another important point when comparing with the experimental data set is that the measurements are not sufficiently resolved to capture the full flame structure, especially in the high gradient regions near the burner, where most of the combustion takes place. This can be seen in Figure 2.7 where the measured radial profiles of temperature are all rather flat even in the region of the strongly swirled flame region.

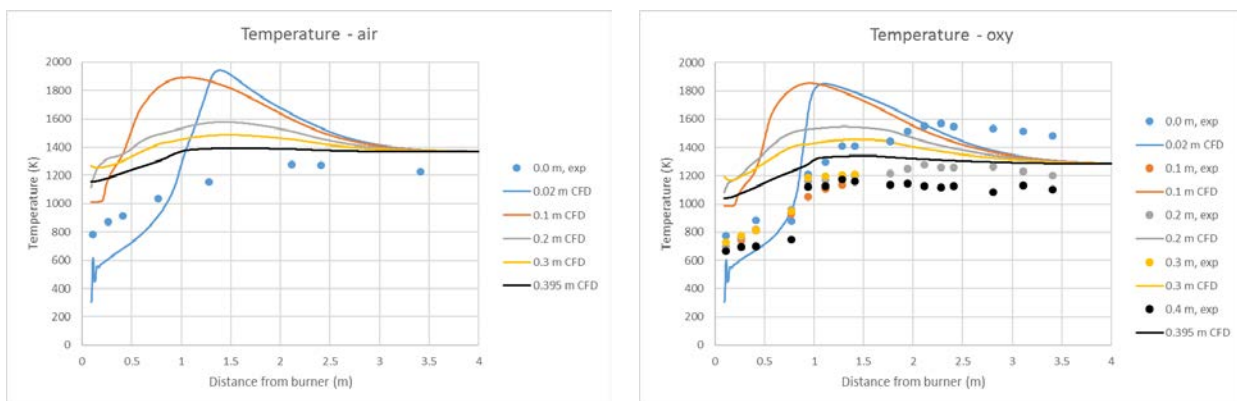


Figure 2.6: Measured and calculated temperature in air and oxy-fuel cases.

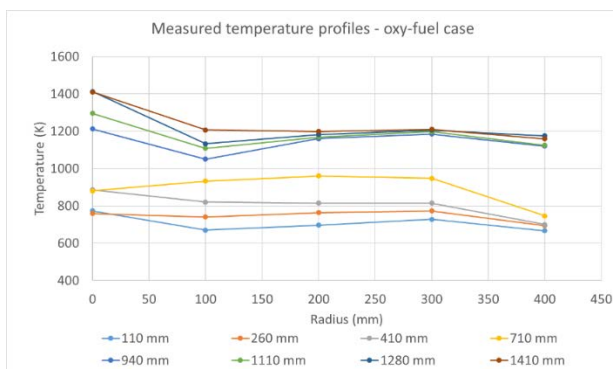


Figure 2.7: Measured temperature radial profiles in oxy-fuel case.

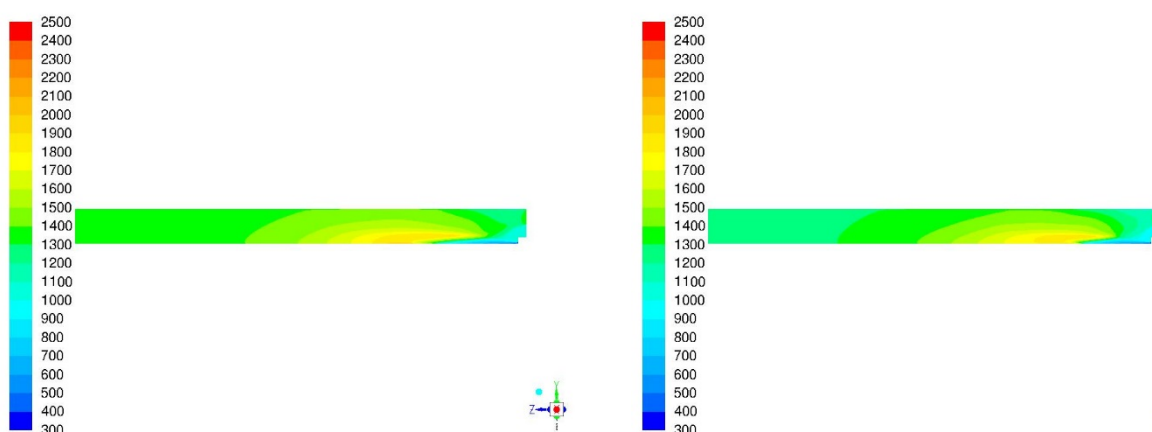


Figure 2.8: Temperature profiles (K) for the air (left) and oxy-fuel (right) cases.

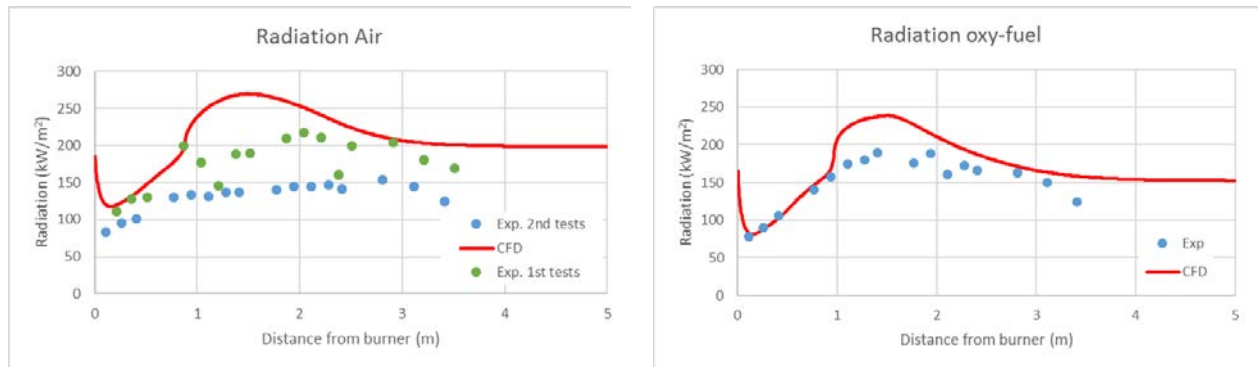


Figure 2.9: Comparison of measured and calculated incident heat radiation.

2.3.2 Incident heat radiation

Calculated and measured longitudinal profiles of incident heat radiation to the wall are shown in Figure 2.9. The incident heat radiation felt at the wall surface is in quite good agreement in the oxy-fuel case, where both the shape and the quantitative values are in good match. The agreement seems to fail between experiments and simulation in the air case when comparing with the second tests, which was the base of the comparison. However, consider that as described in the previous section, there is a difference of around $30 \text{ Nm}^3/\text{h}$ of unaccounted air (leakage and flame detector) in the CFD inputs, which we believe strongly affect the temperature profiles. In fact, from a volume flow input point of view the CFD simulation of air corresponds more to that of the first test campaign, which had a primary flow of $35 \text{ Nm}^3/\text{h}$ less than in the second test. Figure 2.9 also shows the profile obtained during that first test and the agreement is indeed better.

The most important parameter to use for the clinker kiln in this study is the incident heat radiation profiles along the rotary kiln. Even though the calculated incident heat radiation is somewhat higher than the measured, the distribution of the radiated heat is sufficiently well captured. Indeed, the transition between the near field and the region where the incident heat radiation flattens corresponds well with the location where the measured incident heat radiation falls steeply (due to higher heat losses in the experiments).

2.4 Conclusions of the validation study

CFD simulations of the pilot boiler fitted with the new burner design fired with petcoke in air and oxy-fuel modes as fuel have been achieved with a 3D model set up. A large mesh and long computational time were required to reach full convergence, partly due to the high velocity nozzles. The profiles of species and temperature although capturing the trend show a quantitative mismatch with the experiments, which is attributed to:

- the general tendency of higher combustion rate (reduced mechanism and turbulence model),
- the uncertainty and resolution around the measured dataset,
- the extra air flow rates due to leakages and flame detector (up to 23% unaccounted extra air flow).

Importantly for the overall objectives of the project, the incident heat radiation profiles to the walls are matching the measured profiles both in shape and absolute values relatively well.

Despite some discrepancies, given the limitations in the basis for comparison, the flame structure is generally well reproduced by the CFD and that the model developed is considered validated for simulating the full-scale flames. The present work has allowed to prepare the full-scale cases through improvements in setting: the meshing of the complex geometry, the solid fuel chemistry, the radiation model, and the turbulence model. The major problems were related to numerical anomalies and convergence issues such as mass balance errors through the calculation domain and the use of petcoke and its low volatiles levels.

3 METHODOLOGY FOR THE OPTIMIZATION PROCEDURE

The objective of the CFD simulation work in WP7 is to provide the input conditions at the rotary kiln that satisfies the BAT heat radiation to the material. The input conditions are a specification of the amount of gas and its composition in the different sections of the kiln and burner. On the one hand, the flame generated must provide a stable flame and a defined heat radiation profile to the clinker, on the other hand, the gas input and output streams of the rotary kiln must fulfill the overall process constraints set by the clinker cooler downstream and the calciner upstream respectively. Therefore, the rotary kiln input conditions are then used in the process modelling (PM) work in WP6 to ensure a good match with the overall cement making process. The recommended set of data reported in this report are therefore the result of an iterative optimization procedure that is described here.

To understand the chosen procedure, it is important to be aware of the differences in the modelling tools used and highlighted in Figure 3.1. The PM (WP6) covers the whole cement making process from raw material to the final product, in which the rotary kiln is one process through which mass and energy balance is calculated. In the rotary kiln the clinker undergoes chemical and physical transformation as a result of the intense heat it receives during the travelling time. The rotary kiln is modelled in 1D and discretized in 40 elements in which a given heat radiation profile is imposed to the material. The heat profile is defined from inlet mass flows and enthalpy of the fuel, primary and secondary gas streams, and coarse flame geometrical characteristics. In contrast, the CFD simulation (WP7) only simulates the rotary kiln, but solves all the fluid dynamic equations, including turbulence and chemical kinetics of the combustion process. These equations can only be solved at the microscale where mixing and combustion occurs. Therefore, the rotary kiln is simulated in 3D and discretized in 16 million cells in this case and all details of the burner geometry and boundary conditions in all directions must be included.

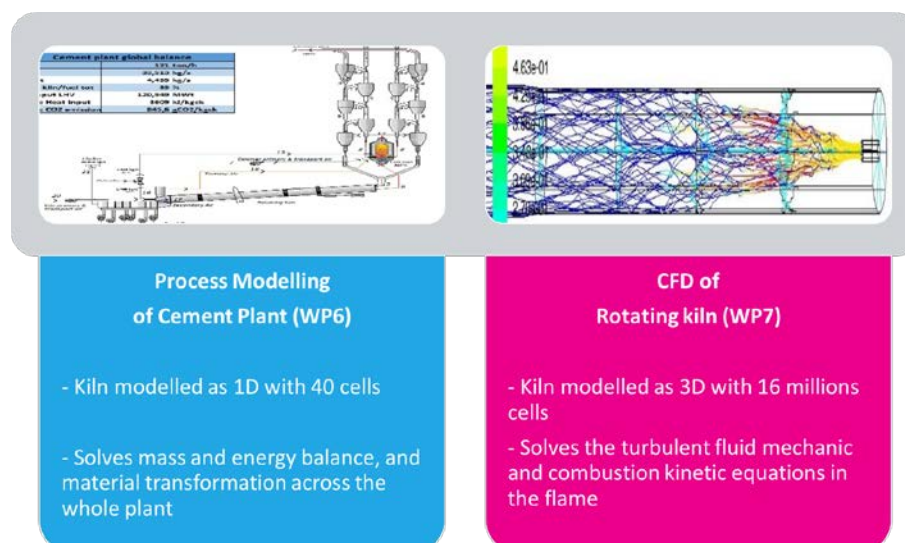


Figure 3.1: The two modelling tools used in the optimization procedure.

Both numerical tools give a material surface incident heat radiation profile along the length of the rotary kiln as an output, but because of the obvious differences in resolution and models used, these profiles can only be compared qualitatively. Besides, for one given set of inlets in the

PM, there are many possibilities to distribute the primary gas at the burner as will be described in a later section. A procedure for optimizing the rotary kiln process based on the two modelling tools has therefore been developed, in which both simulations have as objective to find a solution for the material heat radiation profile in the oxy-fuel case that matches that of the reference air case. The procedure is described as a flowsheet diagram in Figure 3.2, where three criteria must be fulfilled for the CFD simulations of the oxy-fuel case:

- Achievement of a stable oxy-fuel flame and complete combustion
- Rotary kiln integrated heat radiation to the material is within $\pm 1\%$ of that in the reference air case
- Flame region integrated heat radiation to the material is within $\pm 10\%$ of that in the reference air case

Failure to achieve one of these criteria requires finding another set of input conditions at the burner and rotary kiln inlets. Upon success, the corresponding set of inlet conditions and flame characteristics are transferred to WP6 for the PM. The transfer is made manually as PM and CFD are not numerically linked together. The iteration process is considered optimized when the PM results achieved are deemed satisfactory.

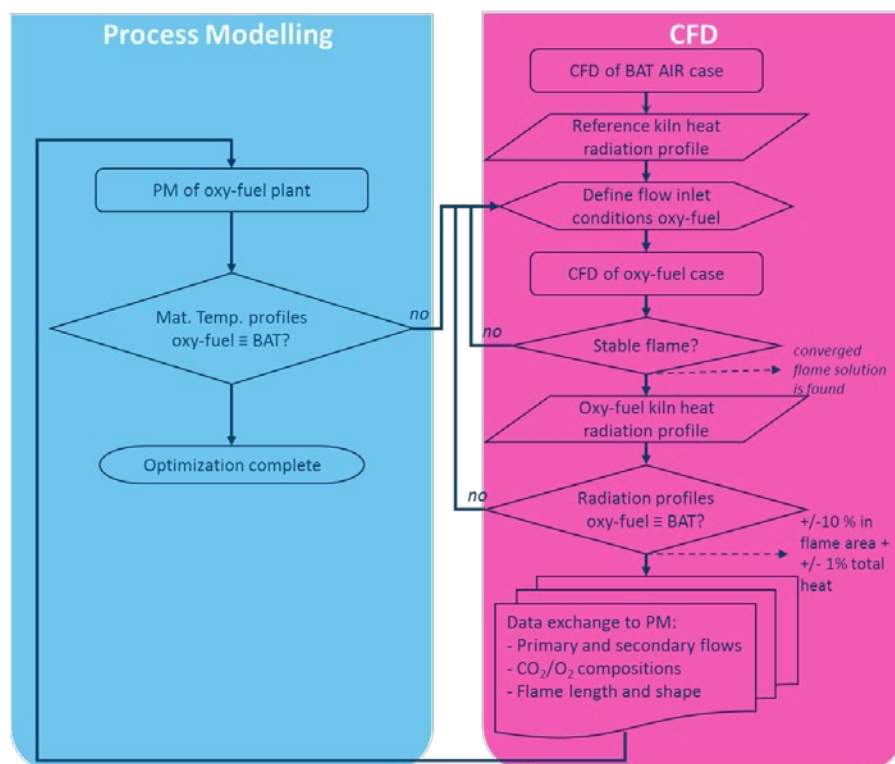


Figure 3.2: Methodology for process optimization.

The definition of the inlet flows into the rotary kiln is not entirely free and is subject to two types of constraints, one is limited by the burner hardware design assigned by the supplier and partner TKIS, the second by the overall process assigned by the partner VDZ and the framework case. The set of constraints is summarized in Table 3.1, a more detailed definition of all streams and their input location is given in the next section.

Table 3.1: Constraints on the rotary kiln inlet conditions.

Parameter	Constraint
O ₂ % in primary stream	None
CO ₂ /O ₂ composition in carrier stream	O ₂ : 0 % - 35 % by vol. (balance CO ₂)
Primary / secondary flow	0.1 – 0.15
Primary CO ₂ flow rate	No limitations, but overall efficiency will decrease with an increase of cold primary flow
Secondary CO ₂ flow rate	34,000 to 40,000 Nm ³ /h
Total primary flow rate	None
Overall rotary kiln excess O ₂	1 - 3 % O ₂ in dry flue gases by vol.
Burner swirl angle	None
Velocities at burner outlets	
Nozzles	150 – 250 m/s, preferably greater than 200 m/s
Secondary	3 – 6 m/s
Carrier gas	15 – 20 m/s
Burner hardware	During the optimization step, a suggestion for burner hardware modification (nozzle size) may be made if a solution does not match the current burner specs

4 NUMERICAL SETUP

4.1 Cement rotary kiln CFD model

The flow and combustion in the cement rotary kiln have been simulated using ANSYS Fluent 17.2. The model meshed is delimited at its back end by a large secondary gas entry and a burner placed at the centerline of the domain, a free gas outlet at the front end of the rotary kiln and a cylinder shaped kiln bounded by a solid wall. The burner used in this study is the CEMCAP partner ThyssenKrupp supplied design under the name of POLFLAME and shown in Figure 4.1. Part of the primary gas stream is used to transport coal through an annular section and another part goes to the 10 adjustable swirl high velocity nozzles to form the flame stabilization zone. The symmetry of the domain allows to simulate only 1/10th of the rotary kiln, with only one nozzle placed at the center of the domain cross section as shown in Figure 4.1. Periodic boundary conditions are set on each sides of the simulated domain. The circular nozzle has been modeled as a trapezoid with the same area. The simulation starts from the outlets of the burner to which a velocity profile with a given swirl is imposed. The burner face picture of Figure 4.1 shows the presence of different ports inside the high velocity nozzles region used for burner ignition and flame monitoring. These ports are not reproduced in the CFD model and are replaced by a solid wall.

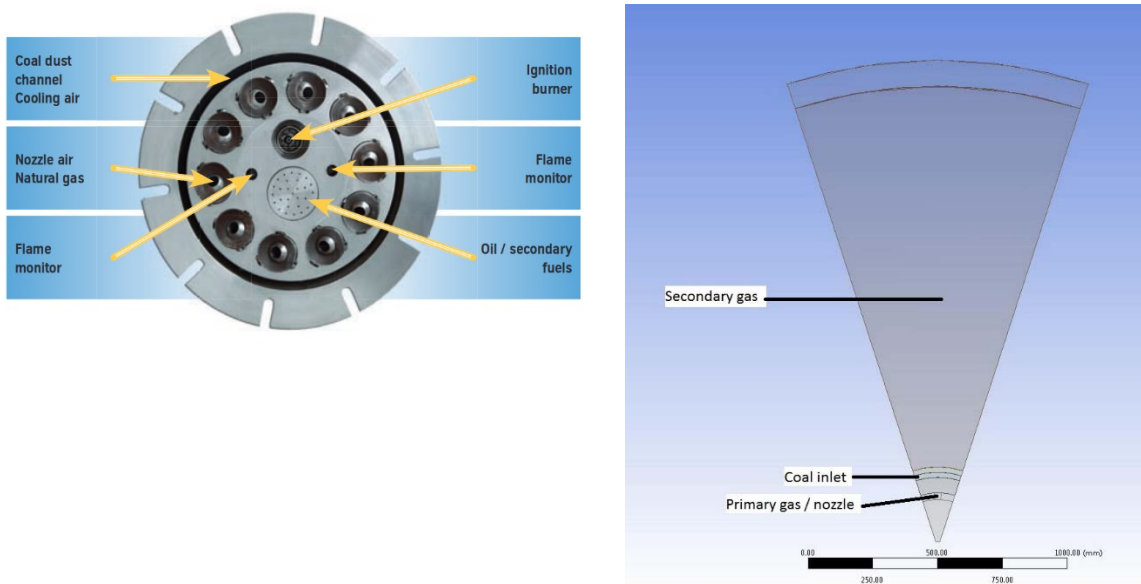


Figure 4.1: ThyssenKrupp POLFLAME burner (left) and its CFD model in the rotary kiln (right).

Burner parameters were based on the current burner design supplied by TKIS [3] where priority is given to keeping the flow velocities at each outlet within a certain range (cf. Table 3.1) as these are detrimental to the desired operation of the burner (impulse and swirl effect). The flow inputs parameters were refined during the optimization procedure described in section §3 within the range given in Table 3.1.

The rotary kiln model dimensions shown in Figure 4.2 has been setup according to TKIS inputs. The rotary kiln is 60 m long with inner diameter of 3.76 m, except in the sintering zone (first 20 m from the burner end of the rotary kiln) where the coating thickness increases (100 mm) reducing the diameter to 3.56 m. Because only a 1/10th of the section is simulated, it is not

possible to include both the refractory wall and the part covered by clinker material as outer boundaries of the rotary kiln. Therefore, in these simulations the boundary condition is set as clinker material in order to capture the correct heat transfer properties between the flame and the material. This assumption should not have a large impact on radiation properties since the emissivity and C_p of refractory walls and those of the clinker are close. Another simplification made in the simulations, is the absence of rotation since the clinker is not modelled as a separate phase.

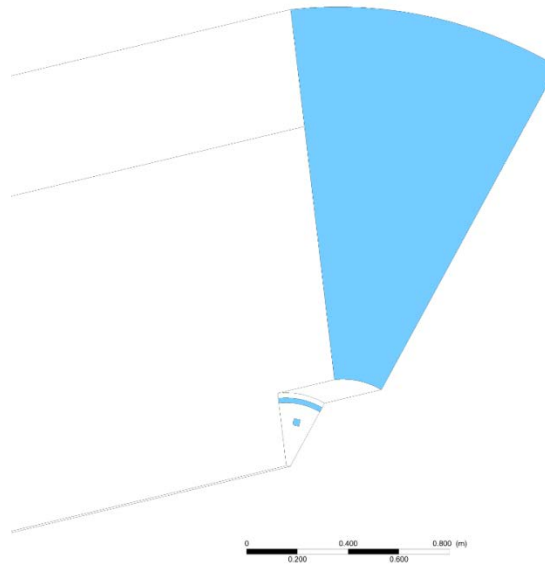


Figure 4.2: Rotary kiln model domain and gas stream inputs (light blue surfaces).

To get a Cartesian grid, the center of the combustion chamber (5 cm diameter) was cut off. This is equivalent to having a 5-cm rod in the center of the combustion chamber. The wall shear stresses on this surface was set to zero. The resulting mesh consisted of 1,648,500 cells. All inlets were set up as mass-flow inlets, while the outlet was set as a pressure outlet. The boundary material temperature in the rotary kiln was specified as a distance along the rotary kiln dependent polynomial function through a User Defined Function (UDF). The polynomial function was fit to the material top surface temperature profile from the CEMCAP framework document [4] and shown in Figure 4.3. Some simulations with an adiabatic boundary were also performed. Note that the very first simulations (before the optimization procedure described earlier started) were based on a different temperature profile.

4.2 Fuel and combustion model

The different models used in the simulations are listed in

Table 4.1. The coal particle distribution is handled through a Rossin-Rammler size distribution method. The combustion model considers coal particles to devolatilize first and then volatiles and char burn. In addition, to the default one-step reaction for volatiles available in the CFD code, six additional reactions have been included in order to have a better accuracy on the combustion behavior in oxy-fuel mode, particularly for the CO kinetics which is known to be limiting. The seven chemical reactions are:

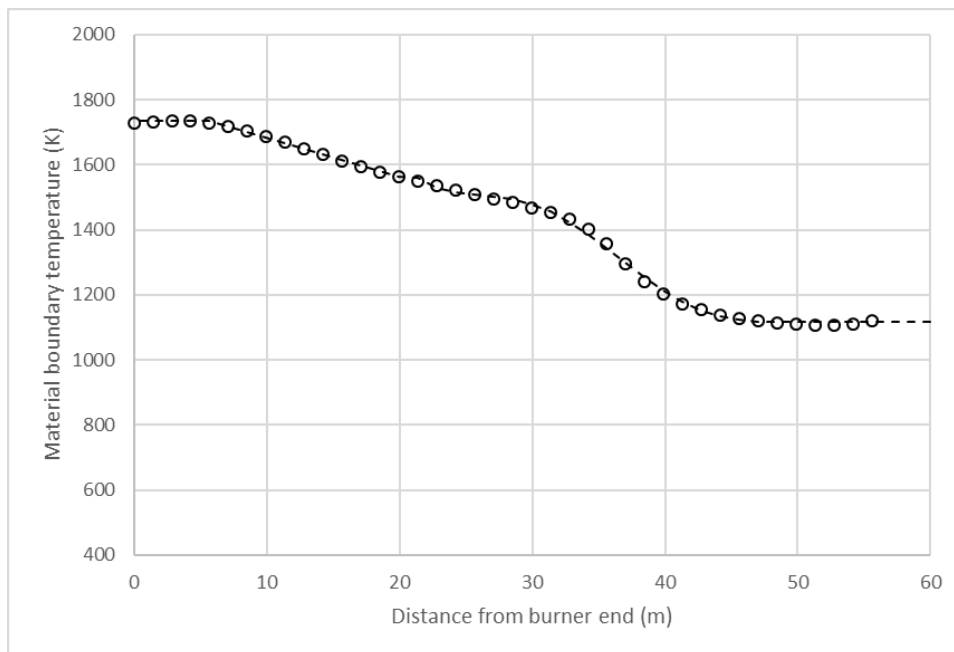


Figure 4.3: Material temperature profile used as boundary condition in CFD simulations (symbols: data from the CEMCAP Framework document [4]; dashed line: polynomial fit used as UDF in the CFD domain).

1. $\text{Volatiles} + 2.01\text{O}_2 \rightarrow 1.2\text{CO}_2 + 2.2\text{H}_2\text{O} + 0.02\text{N}_2 + 0.02\text{SO}_2$
2. $\text{H}_2 + 0.5\text{O}_2 \rightarrow \text{H}_2\text{O}$
3. $\text{CO} + 0.5\text{O}_2 \rightarrow \text{CO}_2$
4. $\text{CO} + \text{H}_2\text{O} \rightarrow \text{CO}_2 + \text{H}_2$
5. $\text{C(s)} + 0.5\text{O}_2 \rightarrow \text{CO}$
6. $\text{C(s)} + \text{CO}_2 \rightarrow 2\text{CO}$
7. $\text{C(s)} + \text{H}_2\text{O} \rightarrow \text{H}_2 + \text{CO}$

Equations 1 – 4 are gas phase combustion reactions, while equations 5 - 7 are heterogeneous reactions to model char burnout. The 4 gas phase reactions are modelled through the Eddy Dissipation Concept model. The reactions leading to SO_2 and N_2 are only present in equation 1 and are produced as soon as the solid particle has devolatilized and starts to burn.

Table 4.1: Models used in the CFD

Turbulence	k-omega SST
Chemistry	Species transport, Finite rate/Eddy-Dissipation, 7 reactions, ideal gas
Radiation	Discrete Ordinates and Weighted Sum of Gray Gases Model
Solver	Pressure based Coupled solver with Pseudo-transient model enabled
Rotary kiln material boundary conditions	Temperature profile for BAT air reference case (cf. Figure 4.3)

Properties for the coal used in the simulations are listed in Table 4.2. Note that the framework document does not impose a particle size distribution for the coal. In order to simulate the effect

of clinker dust heavily present in real rotary kiln, inert particles with properties given in Table 4.3, were introduced together with the secondary gas stream at a rate of 0.28 kg/s (1 t/h) [5].

Oxidizer and inert gas are injected at the burner gas inlets: high velocity nozzles and fuel carrier which in the process are coming from the condenser and the Air Separation Unit (ASU), and at the back end of the rotary kiln as secondary gas coming from the clinker cooler. Further details on composition and conditions of these streams are described in the next section.

Table 4.2: Coal properties.

Property (Units)	Value
HHV (J/kg)	27,150
Volatiles (% by mass)*	27
Fixed C (% by mass)*	56
Ash (% by mass)	16.5
Moisture (% by mass)	0.5
Coal size (μm)*	100 - 400
Coal ultimate analysis (water and ash free):	
C (% by mass)	83.15
H (% by mass)	4.82
O (% by mass)	10.85
N (% by mass)	0.58
S (% by mass)	0.60
Density (kg/m^3)	1400
C_p (J/kg K)	1680
Combustion model parameters:	
Particle emissivity (-)	1
Vaporization temperature for volatiles (K)	600
Binary diffusivity (m^2/s)	4.10^{-5}
Particle scattering factor (-)	0.9
Swelling coefficient (-)	1.4
Reaction of heat absorbed by solid (%)	30
Constant rate devolatilization model (1/s)	12
* Not specified in the framework document	

Table 4.3: Clinker dust properties.

Property (Units)	Value
Density (kg/m^3)	1400
C_p (J/kg K)	Polynomial [6]
Particle emissivity	0.9
Particle scattering factor	0.9
Inlet velocity (m/s)	As in secondary flow
Particle diameter (μm)	150
Particle inlet temperature (K)	1073
Mass flow rate (kg/s)	0.28

5 RESULTS AND DISCUSSION

The rotary kiln inlet flow parameters used in the reference case and in the last three oxy-fuel cases of the optimization process described in the methodology (cf. §3) are shown in Table 5.1. Note that these parameters are significantly different than those in the 500 kW prototype tests made at the University of Stuttgart [1] because the Stuttgart facility had local constraints (preheating capacity and existing size of the boiler amongst other).

Table 5.1: CFD simulations inlet properties.

Combustion cases:		AIR-Ref.	OXY-Round 3	OXY-Round 4	OXY-Round 6
Primary gas					
Volume flow rate	Nm ³ /h	5,100	4,068	4,500	4,500
Temperature	K	323	323	323	323
Composition					
N2 or CO2		N2	CO2	CO2	CO2
O2	% by vol.	21	60	60	60
N2 or CO2	% by vol.	79	40	40	40
Swirl degree	angle	20° tangential	40° tangential	30° tangential	30° tangential
Velocity	m/s	250	200	221	221
Carrier gas					
Volume flow rate	Nm ³ /h	4,040	1,600	1,600	1,050
Temperature	K	323	323	323	323
Composition					
N2 or CO2		N2	CO2	CO2	CO2
O2	% by vol.	21	30	30	18
N2 or CO2	% by vol.	79	70	70	82
Velocity	m/s	38.3	15.2	15.2	10.0
Fuel					
type		coal	coal	coal	coal
mass flow rate	kg/s	1.469	1.469	1.469	1.469
stoichiometric O2 mass	g_O2/g_fuel	2.070	2.070	2.070	2.070
Primary + Carrier					
Volume flow rate	Nm ³ /h	9,140	5,668	6,100	5,550
Temperature	K	323	323	323	323
Composition					
N2 or CO2		N2	CO2	CO2	CO2
O2	% by vol.	21.0	51.5	52.1	52.1
N2 or CO2	% by vol.	79.0	48.5	47.9	47.9
O2	Nm ³ /h	1,919	2,921	3,180	2,889
CO2 or N2	Nm ³ /h	7,221	2,747	2,920	2,661
available combustion O2	g_O2/g_fuel	0.518	0.789	0.859	0.780
Secondary gas					
Volume flow rate	Nm ³ /h	29,090	32,714	36,000	28,126
Temperature	K	1073	1073	1073	1273
Composition					
N2 or CO2		N2	CO2	CO2	CO2
O2	% by vol.	21.0	18.0	18.0	20.8
N2 or CO2	% by vol.	79.0	82.0	82.0	79.2
Velocity	m/s	3.7	4.2	4.6	4.3
Flue gas composition					
O2	% dry by vol.	1.1	2.8	4.6	3.0
N2	% dry by vol.	80.8	0.1	0.0	0.1
CO2	% dry by vol.	18.1	97.1	95.3	96.9
H2O	% wet by vol.	6.0	6.1	5.5	6.9

The Oxy-Round 4 case fulfilled the criteria defined in the methodology (cf. §3) regarding flame stability and heat distribution in the rotary kiln, and was therefore considered to be an optimized oxy-fuel case from the CFD's perspective. The combustion is complete as can be shown by the mass fraction of major species at the outlet plane of the CFD simulation domain being equal to that from the mass balance with full conversion (cf. Table 5.2). Its corresponding inlet conditions were passed on to the process modelling group in WP6 of the CEMCAP project, and a final loop in the iteration process led to the proposal of a further optimized Oxy-Round 6 which needed be controlled by CFD as described in Figure 3.2. The outlet results from the new Oxy-Round 6 CFD are also shown in Table 5.2 and all the criteria were also positive, thus fully closing the optimization procedure. The only results presented in the following are those of the optimized Oxy-Round 6 and air reference cases. A total of 16 cases have been run with the purpose of improving the simulation quality.

Table 5.2: Mass fraction of species at the rotary kiln outlet for selected cases.

	Air (Ref Case)		Oxy-Round 4		Oxy-Round 6	
	CFD outlet	Mass balance	CFD outlet	Mass balance	CFD outlet	Mass balance
Volatiles	0	0	1.0E-10	0	8.4E-13	0
O₂	0.0105	0.0100	0.0197	0.0326	0.0210	0.0205
CO₂	0.2484	0.2486	0.9534	0.9426	0.9483	0.9486
H₂O	0.0356	0.0359	0.0259	0.0239	0.0295	0.0297
SO₂	0.001	0.001	0.0007	0.0007	0.0008	0.0008
CO	3E-07	0	8E-11	0	0.0000	0
H₂	3E-11	0	9E-14	0	0.0000	0
N₂	0.7046	0.7046	0.0003	0.0003	0.0004	0.0004
Temp. (K)	1065		1111		1079	

5.1 Flame dimension

Two flame size characteristics are necessary as input to the PM: the flame length and shape. There are several means for measuring flame length experimentally, it can be done visually through flame observable intensity or by measuring a species or temperature profile along the flame centerline. In this study, we define the flame length at the point in the streamwise direction where the decreasing mean temperature profile crosses 1400°C. This is also the definition that was used in the ECRA CCS project, and it corresponds to the inflexion point in the temperature decay. Results for the reference and the last two oxy-fuel cases are given in Table 5.3. The flame shapes obtained are qualified as triangular for the flames investigated as can be seen in the example given in Figure 5.1. The triangular aspect is a result of the expanding flow generated by the strong swirl.

Table 5.3: Flame length results.

Case	Flame length
Air Ref	17.0 m
Oxy Round 4	16.0 m
Oxy Round 6	16.8 m

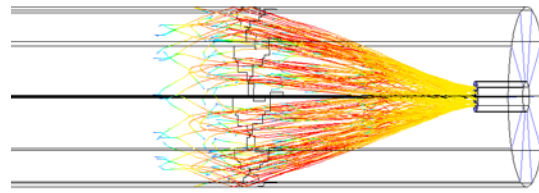


Figure 5.1: Char particles trajectories and mass fraction in case Oxy-Round6 showing the "triangular" flame shape in the near burner region.

5.2 Flame radiation properties

Surface incident heat radiation at the material is a critical characteristic of the rotary kiln flame as the product quality strongly depends on it. Figure 5.2 shows the surface incident heat radiation profiles for the reference air case and two optimized oxy-fuel cases. From around 20 meters to downstream the rotary kiln end (material inlet), there is little variation between the cases because this region is mainly composed of well mixed hot gases, homogenous in composition and temperature. The differences are more marked in the first 20 meters region corresponding to the flame where the distribution of temperature and species are controlled by the burner inlet conditions in terms of inlet velocity, composition, and degree of swirl as will be seen in the next section.

The rotary kiln integrated incident heat radiation to the material are deviating by -0.8 % and 2.1 % from that of the reference case for the optimized oxy-fuel cases Oxy-round 4 and Oxy-round 6 respectively. When integrated over the near flame region the corresponding deviations are -7.9 % and 2.0 %. These deviations are within the criteria set in §3 of 1 % and 10 % for the Oxy-Round 4, but higher for the overall flame for Oxy-round6 (2.1 % against 1 %). This deviation is however accepted as it is due to a higher secondary gas temperature. Table 5.1 shows the differences in the primary gas stream between the reference air and oxy-fuel cases, showing that the total available gas in the primary stream (i.e. primary gas + carrier gas) is one third lower in the oxy-fuel case. Most of the flow reduction has been applied to the carrier gas stream because it is important to achieve high velocity at the nozzles for the flame stabilization. The degree of swirl has been increased in order to compensate for the lower velocity. Another noticeable difference is the oxygen concentration at the nozzle which is as high as 60 % in the oxy-fuel case, although the oxygen concentration "seen" by the coal is at best 52 % when taking into account the coal carrier gas. The results show that the same burner can be used in air and oxy-fuel modes, making it flexible for mode shifting purposes and a good retrofit hardware, but it is at the expense of significant variation in inlet conditions.

It is seen in Figure 5.2 that the reference case material receives a higher peak radiation intensity than in the oxy-fuel case, being the location where most of deviation in the integrated heat radiation is. Attempt to further reduced the deviation would have forced one or several of the following measures:

- Further enrich the primary stream in oxygen.
- Further increase the swirl degree.
- Further decrease the carrier flow velocity (in order to increase the velocity in the primary stream nozzle).

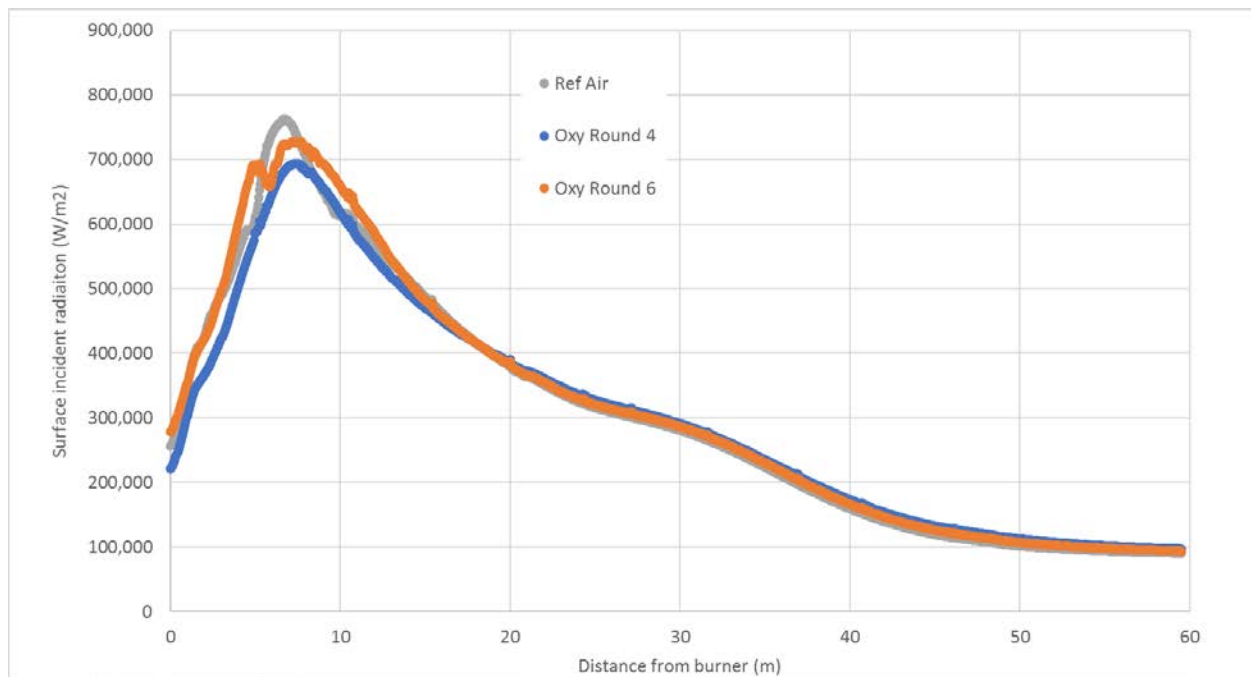


Figure 5.2: Surface incident heat radiation profile at the rotary kiln boundary for three cases.

Such modifications would result in what is considered as a too large deviation from the burner originally intended conditions and were therefore not pursued since the defined criteria for acceptance of the optimized cases were already achieved. Burner hardware modifications would also be a solution, but has been overlooked here because of the planned retrofit application for this study. Finally, another parameter that could be varied to improve the fit is the primary gas temperature, as will be explained in a latter section, but is however not free for modification (cf. constraint definition of Table 3.1).

5.3 Near burner flame characteristics

The previous section showed the results of the optimization procedure from a process point of view with clearly defined criteria that the oxy-fuel case should fulfill. These criteria are macroscopic effect of the flame on the material, however the oxy-fuel flame obtained has strong structural difference as compared to the reference case. In this section we highlight the differences in the near region from the burner, that is the region where the flame is stabilized in a complex turbulent fluid dynamic pattern.

5.3.1 Temperature field

The temperature maps of Figure 5.3 show the structure of the flame with a slightly more expanding flame front in the oxy-fuel case and a stabilization of the flame at approximately the same distance from the burner. The most striking difference is in the peak temperature which reaches a higher value in the air case (2360 K against ca. 2239 K) although the primary gas oxygen composition in the oxy-fuel case is as high as 60% in the oxy-fuel case (cf. Table 5.1). This result appears as a paradox knowing the strong dependence of the adiabatic flame temperature on oxygen concentration in the oxidizer. For the sake of comparison, methane burning in these two oxidizer compositions would have a difference in adiabatic flame temperature of nearly 475 K in favor of the oxy-fuel case. The observed peak temperature difference is truly responsible for the higher peak heat radiation felt by the material also

observed in Figure 5.2. To understand this phenomenon it is necessary to look deeper in the flame structure and analyze how combustion evolves from the injection of cold coal particles to fully burned.

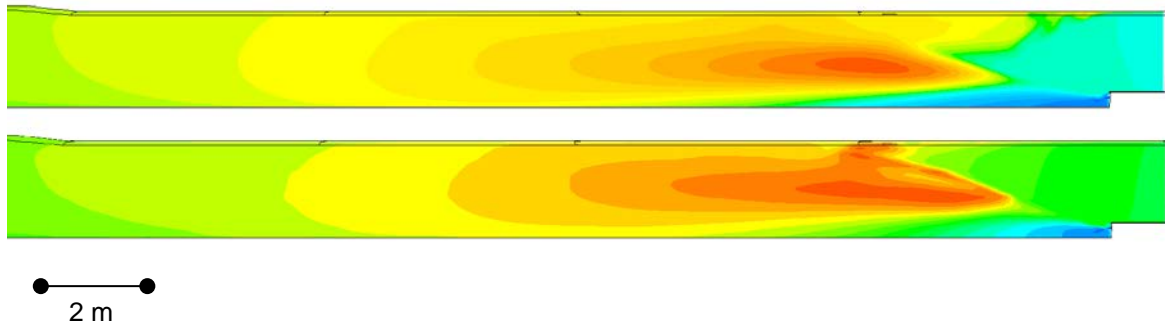


Figure 5.3: Contour maps of temperature (K) in the plane crossing the nozzle centerline. Air reference (top) and oxy-round 6 (bottom) cases with respectively 2360 K and 2239 K peak values.

The Figure 5.4 is a three-dimensional representation of the flame temperature field highlighting the non-homogeneity of the flame in the radial and tangential directions up to at least 5 m downstream the burner, where the presence of the swirling high velocity jet can be deduced. As already in observed in Figure 5.3, the air flame reaches homogeneity sooner because all non-fuel gas streams involved have the same composition. This point also shows that one should be careful in discussing longitudinal cross-section at a given radial angle.

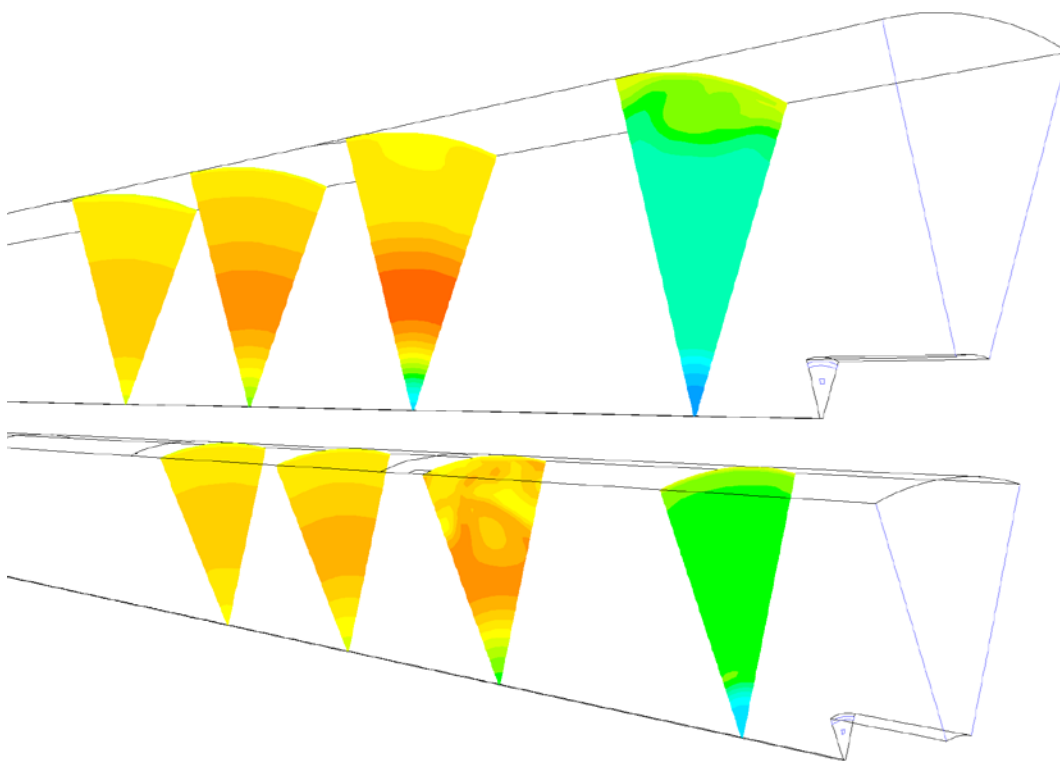


Figure 5.4: Temperature (K) cross section maps at 2 m, 5 m, 7.5 m, and 10 m from rotary kiln gas end. Air reference (top) and oxy-round 6 (bottom) cases (same color scale as in Figure 5.3).

5.3.2 Species

Oxygen concentration maps are given in Figure 5.5 showing clearly the more complex oxidizer distribution at the beginning of the rotary kiln in the oxy-fuel case, due to the strong difference in inlet compositions of the three gaseous mixtures (primary, carrier, and secondary streams). Corresponding maps of CO concentration are shown in Figure 5.6. There the differences are also very much marked due to the particular chemistry of CO₂. The three heterogeneous reactions of char which are modelled in these simulations (equations 5 to 7 in §4.2) are strong producers of CO, particularly when CO₂ is present at large partial pressures in the so-called Boudouard reaction (equation 6) which net production reaction rate is two orders of magnitude larger in the oxy-fuel case. This dependency was also clearly observed in the 500 kW pilot tests at varying oxygen concentration in the primary gas (Figure 5.8).

Near the kiln boundary, a high CO concentration spot can be observed and can be explained by the flow dynamic pattern of the coal particles shown in Figure 5.1. It is seen that part of the char formed during devolatilization has not gasified completely before their trajectories hit the material boundary. In addition, the CO concentration cross section maps of Figure 5.7 show that at that distance from the burner, the flow and species distributions are still under the strong effect of the swirling motion and not homogeneously mixed in the radial direction. The high CO spot at the solid surface is therefore due to a quenching of the homogeneous CO reduction reactions.

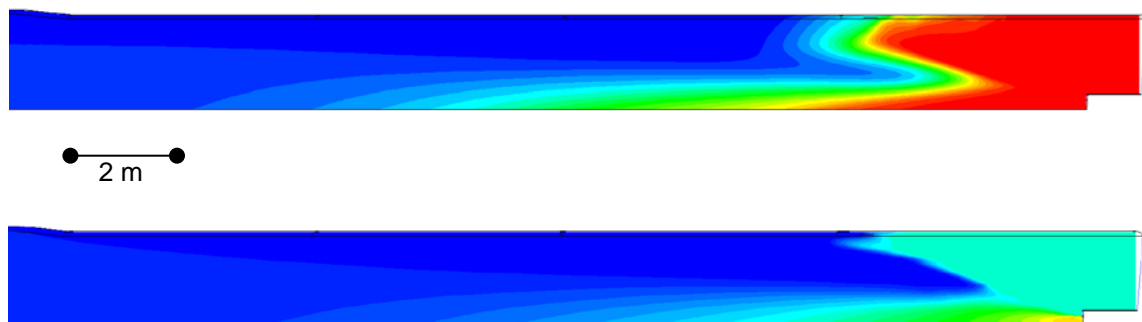


Figure 5.5: Contour maps of O₂ volume fraction in the plane crossing the nozzle centerline. Air reference (top) and oxy-round 6 (bottom) cases.

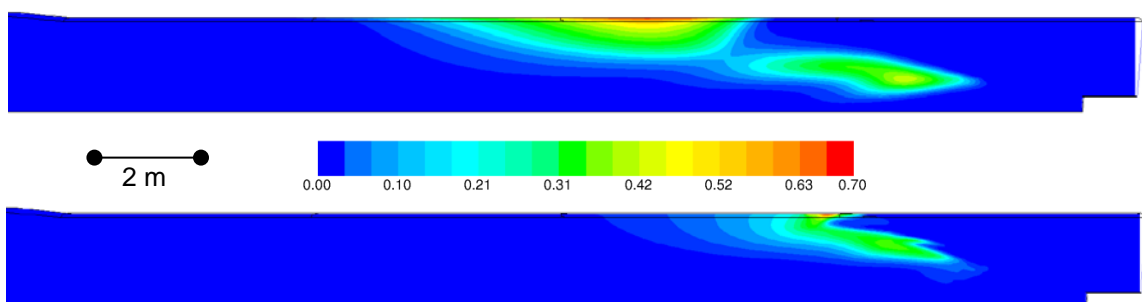


Figure 5.6: Contour maps of CO volume fraction in the plane crossing the nozzle centerline. Air reference (top) and oxy-round 6 (bottom) cases.

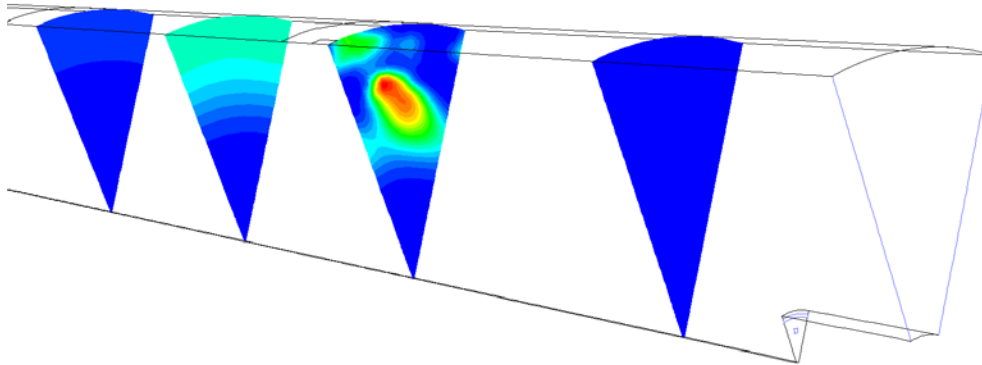


Figure 5.7: CO (volume fraction) cross section maps at 2 m, 5 m, 7.5 m, and 10 m from rotary kiln gas end. Oxy-round 6 case.

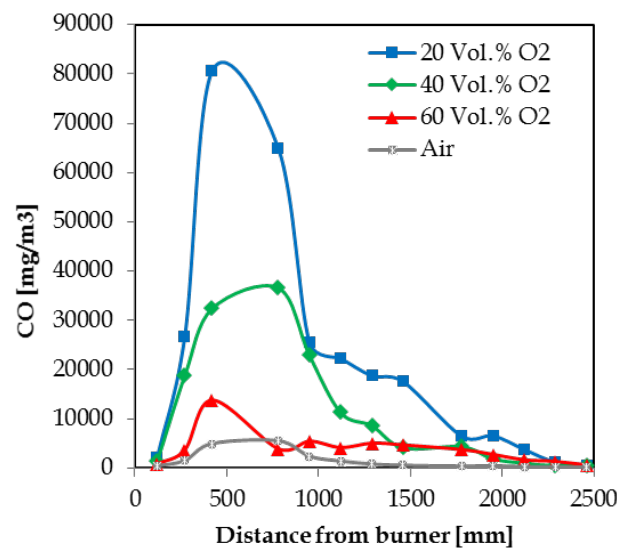


Figure 5.8: CO concentrations dependency on primary gas composition measured at the lignite fired 500 kW University of Stuttgart facility as part of the CEMCAP project.

5.4 Discussions

5.4.1 Temperature paradox

As highlighted in section §5.3.1, the higher peak temperature attained in the air case constitutes a paradox given the much higher oxygen concentration in the primary oxidizer composition. The oxygen concentration fields shown Figure 5.5 give a possible explanation for that phenomenon. Indeed, the oxygen concentration in the range of 60 % are not to be seen anywhere in the domain, but at the primary gas outlet plan. The primary flow becomes very soon diluted, first by the carrier gas surrounding the coal particles, and then mostly by the large amount of secondary

gas only containing 20.8 % O₂ in CO₂. The temperature map shows that the combustion reactions are mostly stabilized at around 2.4 meters away from the burner and at approximately 1.4 meter off the centerline, giving enough time for the primary flow to be diluted to an O₂ concentration of ca. 25 – 29 %. At these concentrations, the calculated adiabatic flame temperature in CO₂ is indeed lower than in air due to the higher calorific value of CO₂, explaining thus the apparent temperature paradox.

5.4.2 Flame stabilization and heat radiation profile

The combustion stabilization zone is delayed from the burner as a result of the time needed for the coal to reach devolatilization temperature as seen in the plot of char mass fraction of Figure 5.1. It implies that increasing the primary gas temperature, while keeping all other inlet variables constant, would result in an increase of peak temperature (hence gas heat radiation rate to the material) by favoring combustion of coal in a region with higher O₂ concentration. This point highlights the importance of a correct model for devolatilization.

6 CONCLUSIONS AND FURTHER WORK

Following an agreed optimization procedure, several CFD simulations have been performed for the reference BAT air case and various oxy-fuel cases. The optimization led to the set of input parameters (inlet flow rates, temperatures, and compositions, swirl angle) summarized in Table 6.1 for the optimized oxy-fuel case that generates a flame in the rotary kiln delivering a heat radiation profile to the material similar to that in the reference case. In order to provide a similar heat radiation profile, the oxy-fuel flame length and temperature distribution in the rotary kiln are different than that in the reference air case due to the different fluid properties. According to the simulations, the POLFLAME burner is a burner that can be used for retrofit application, where only the swirl angle at the high velocity nozzles (which is not an input for the process modelling) needs be adjusted when shifting from air to oxy-fuel mode, and the burner hardware is designed to do so.

Table 6.1: Summary of the optimized oxy-fuel case (Oxy-Round 6).

Parameter	Oxy-Round 6
Primary* flow rate	5,550 Nm ³ /h
Primary* flow CO ₂ /O ₂ composition	47.9 % / 52.1% by vol.
Primary* flow temperature	323 K (50°C)
Secondary flow rate	28,126 Nm ³ /h
Secondary flow CO ₂ /O ₂ composition	79.2 % / 20.8 % by vol.
Secondary flow temperature	1273 K (1000°C)
Flame length	16.8 m
Flame shape	Triangular

* including fuel carrier flow

The study performed and presented herein has been customized as to answer the objective of the optimization procedure in parallel with the Process Modelling work - which considers the entire cement making process - for finding an optimized set of inlet conditions at the rotary kiln. A fair balance was found and considered acceptable between the level of detailing and accuracy of the models, and the numerical expense in terms of CPU time and efforts to achieve converging cases. It is recommended that further studies consider air entries in the rotary kiln and the secondary gas stream (through the cooler), such as their effect on NO_x and gas properties to the calciner, hence flue gas cleaning unit, can be better assessed. Further improvements in the CFD setup could also be applied to increase the accuracy of the numerical calculations, and are listed in a non-prioritized order as follows:

- Use of an oxy-fuel optimized gas radiation model;
- Include an improved model for the devolatilization of coal on the flame stabilization region;
- Include an improved model for the particle dispersion;
- Modelling of the clinker chemistry (instead of applied temperature profile);
- Modelling of the clinker as an own phase with a model for the heat and mass rotation controlled mixing in the phase (instead of a fixed wall boundary).

The last two points requires simulation of at least half of the rotary kiln, i.e. a 5 times larger domain than in the present study.

From simulation and the experimental work reported in Deliverable 7.2 and in Deliverable 7.3 it can be concluded, that a burner design with single jets as currently used in many modern kilns is suitable for oxy-firing in cement kilns. A burner design with single jets benefits of a larger surface area for the injection of primary gas in comparison to channel burners. This feature improves significantly the entrainment of secondary gas, which enhances fuel ignition especially important for combustion under high CO₂ partial pressure.

For a greenfield application no special design modification is foreseen. However, it is recommended to install burners with adjustable swirl angle, since it was observed to be a powerful tool in tuning flame formation to obtain similar air-flame characteristics. In case an existing kiln line is to be retrofitted for oxy-fuel firing, a state of the art single jet burner would be recommended. Retrofitting of for example a channel burner is not deemed to be feasible for economic reasons. If the kiln line already has a state of the art burner with single jets and primary gas momentum needs to be adjusted, a nozzle diameter change can be considered. The new nozzle size is determined according to the primary gas design figures.

7 REFERENCES

1. CEMCAP Milestone Report MS7.3: Second kiln prototype burner design available
2. Kühnemuth, D.; Normann, F.; Andersson, K.; Johnsson, F. On the carbon monoxide formation of in oxy-fuelcombustion—Contribution by homogenous and heterogeneous reactions. *International Journal of Greenhouse Gas Control*. 25(2014) pp 33-41.
3. Email communication, dated May 4th, 2017 from E. Willms to WP7 participants (confidential)
4. Figure 3.7 *in*: D3.2-CEMCAP framework for comparative techno-economic analysis of CO₂ capture from cement plants.
5. Email communication, dated June 21st, 2017 from A. Jamali to WP7 participants (confidential)
6. Email communication, dated August 17th, 2017 from A. Jamali to WP7 participants (confidential)